RESEARCH ARTICLE SUMMARY

DEVELOPMENT

Mitochondria metabolism sets the species-specific tempo of neuronal development

Ryohei Iwata†, Pierre Casimir†, Emir Erkol, Leïla Boubakar, Mélanie Planque, Isabel M. Gallego López, Martyna Ditkowska, Vaiva Gaspariunaite, Sofie Beckers, Daan Remans, Katlijn Vints, Anke Vandekeere, Suresh Poovathingal, Matthew Bird, Ine Vlaeminck, Eline Creemers, Keimpe Wierda, Nikky Corthout, Pieter Vermeersch, Sébastien Carpentier, Kristofer Davie, Massimiliano Mazzone, Natalia V. Gounko, Stein Aerts, Bart Ghesquière, Sarah-Maria Fendt, Pierre Vanderhaeghen*

INTRODUCTION: During embryonic development, the temporal sequence of events is usually conserved throughout evolution, but it can occur at very different time scales depending on the species or cell type considered. The human cerebral cortex is characterized by a considerably prolonged timing of neuronal development compared with other species, taking months to years to reach maturity compared with only a few weeks in the mouse. The resulting neoteny is thought to be a key mechanism enabling enhanced function and plasticity of the human brain. Human and nonhuman cortical neurons cultured in vitro or xenotransplanted into the mouse brain develop along their species-specific timeline. This suggests that species-specific developmental timing is controlled by cell-intrinsic mechanisms, but these remain essentially unknown.

RATIONALE: Metabolism and mitochondria are key drivers of cell fate transitions in many systems, including the developing brain. Here, we tested whether they could be involved in the species-specific tempo of cortical neuron development and human brain neoteny.

We developed a system of genetic birth-dating to label newly born neurons with high temporal and cellular resolution, and directly compared the development of human and mouse cortical neurons over time. We profiled, across time and species, mitochondria morphology, gene expression, oxygen consumption, and glucose metabolism. Next, we used pharmacological or genetic manipulation of human or mouse neurons to enhance or decrease their mitochondria function, and determined the consequences on the speed of neuronal development.

RESULTS: We found that mitochondria are initially low in size and quantity in newborn neurons, and then grow gradually as neurons undergo maturation following a species-specific timeline. Whereas in mouse neurons, mitochondria reach mature patterns in 3 to 4 weeks, they only do so after several months in human neurons.

We next measured mitochondria oxidative activity and glucose metabolism in human and mouse developing cortical neurons. This revealed a species-specific timeline of functional maturation of mitochondria, with mouse neurons displaying a much faster increase in mitochondria-dependent oxidative activity than human neurons. We also found that human cortical neurons displayed lower levels of mitochondria-driven glucose metabolism than did mouse neurons at the same age.

Finally, we tested whether mitochondria function affects neuronal developmental timing. We performed pharmacological or genetic manipulation of human developing cortical neurons to enhance mitochondria oxidative metabolism. This led to accelerated neuronal maturation, with neurons exhibiting more mature features weeks ahead of time, including complex morphology, increased electrical excitability, and functional synapse formation. Similar treatments on mouse neurons also led to faster maturation, whereas inhibition of mitochondria metabolism in mouse neurons led to a decrease in developmental rates.

CONCLUSION: Our work identifies a species-specific temporal pattern of mitochondria and metabolic development that sets the tempo of neuronal maturation. Accelerated human neuronal maturation using metabolic manipulation might benefit pluripotent stem cell–based modeling of neural diseases, which remains greatly hindered by protracted neuron development. Tools to accelerate or decelerate neuronal development could allow testing of the impact of neuronal neoteny on brain function, plasticity, and disease. ■

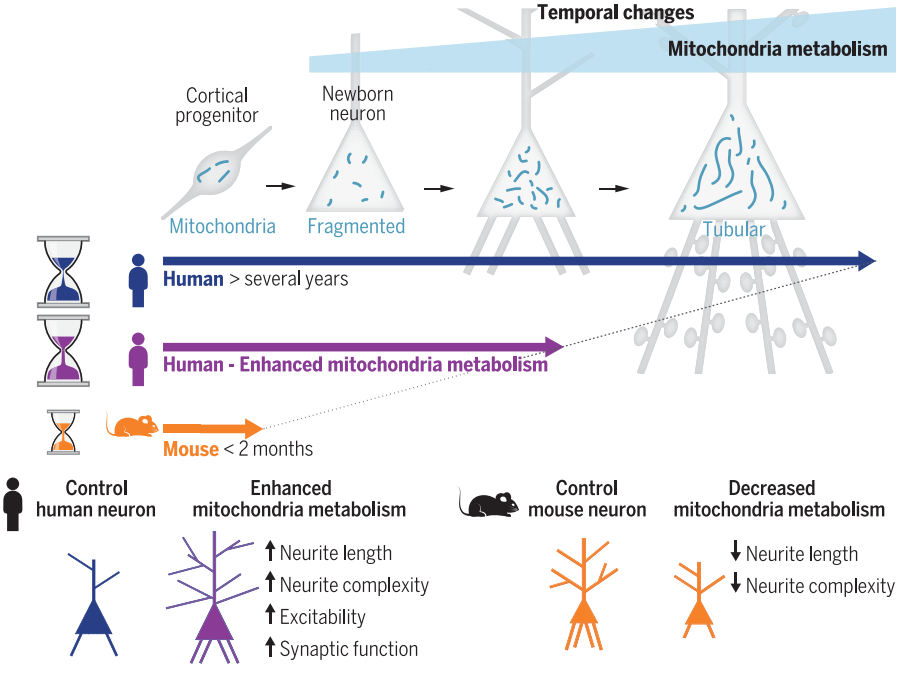

Mitochondria metabolism sets the tempo of neuronal development. Mitochondria dynamics and metabolism display species-specific timelines during cortical neuron development. In newborn neurons, mitochondria are small in number and metabolic activity, and then increase gradually during neuronal maturation. Enhanced mitochondria metabolism in human neurons leads to accelerated maturation, including increased neurite complexity, excitability, and synaptic function. Decreased mitochondria metabolism in mouse neurons leads to decelerated neuronal maturation.

The list of author affiliations is available in the full article online.
*Corresponding author. Email: pierre.vanderhaeghen@kuleuven.be
†These authors contributed equally to this work.
Cite this article as R. Iwata *et al.*, *Science* **379**, eabn4705 (2023). DOI: 10.1126/science.abn4705

READ THE FULL ARTICLE AT
https://doi.org/10.1126/science.abn4705

RESEARCH ARTICLE

DEVELOPMENT

Mitochondria metabolism sets the species-specific tempo of neuronal development

Ryohei Iwata[1,2,3]†, Pierre Casimir[1,2,3]†, Emir Erkol[1,2], Leïla Boubakar[1,2,3], Mélanie Planque[4,5], Isabel M. Gallego López[1,2], Martyna Ditkowska[1,2], Vaiva Gaspariunaite[1,2], Sofie Beckers[1,2], Daan Remans[1,2], Katlijn Vints[2,6], Anke Vandekeere[4,5], Suresh Poovathingal[1], Matthew Bird[7], Ine Vlaeminck[1,8], Eline Creemers[1,8], Keimpe Wierda[1,8], Nikky Corthout[1,9], Pieter Vermeersch[10], Sébastien Carpentier[11], Kristofer Davie[1], Massimiliano Mazzone[12,13], Natalia V. Gounko[2,6], Stein Aerts[1,2], Bart Ghesquière[14], Sarah-Maria Fendt[4,5], Pierre Vanderhaeghen[1,2,3]*

Neuronal development in the human cerebral cortex is considerably prolonged compared with that of other mammals. We explored whether mitochondria influence the species-specific timing of cortical neuron maturation. By comparing human and mouse cortical neuronal maturation at high temporal and cell resolution, we found a slower mitochondria development in human cortical neurons compared with that in the mouse, together with lower mitochondria metabolic activity, particularly that of oxidative phosphorylation. Stimulation of mitochondria metabolism in human neurons resulted in accelerated development in vitro and in vivo, leading to maturation of cells weeks ahead of time, whereas its inhibition in mouse neurons led to decreased rates of maturation. Mitochondria are thus important regulators of the pace of neuronal development underlying human-specific brain neoteny.

Developmental processes display species-specific differences in timeline, or heterochrony, which can lead to divergence in size, cell composition, or organ function (*1*–*3*). Human brain development is characterized by a prolonged timing of maturation of cortical neurons compared with that of other species (*4*). Such neoteny may underlie the enhanced performance of the human brain (*5*). Human and nonhuman primate cortical neurons derived from pluripotent stem cells (PSCs) and xenotransplanted into the mouse brain develop along their species-specific timeline (*6*–*8*), pointing to cell-intrinsic developmental timing mechanisms. Metabolism and mitochondria are drivers of cell fate transitions (*9*–*12*) and maturation (*13*–*15*) in many systems, including the brain (*16*–*21*). Species differences in metabolism at the organism level are linked to developmental growth (*22*, *23*), but whether metabolism influences species-specific developmental tempo remains unclear.

[1]VIB-KU Leuven Center for Brain & Disease Research, 3000 Leuven, Belgium. [2]KU Leuven, Department of Neurosciences & Leuven Brain Institute, 3000 Leuven, Belgium. [3]Université Libre de Bruxelles (ULB), Institut de Recherches en Biologie Humaine et Moléculaire (IRIBHM), and ULB Neuroscience Institute (UNI), 1070 Brussels, Belgium. [4]Laboratory of Cellular Metabolism and Metabolic Regulation, VIB-KU Leuven Center for Cancer Biology, VIB, 3000 Leuven, Belgium. [5]Laboratory of Cellular Metabolism and Metabolic Regulation, Department of Oncology, KU Leuven and Leuven Cancer Institute (LKI), 3000 Leuven, Belgium. [6]VIB-KU Leuven Center for Brain & Disease Research, Electron Microscopy Platform & VIB-Bioimaging Core, 3000 Leuven, Belgium. [7]Clinical Department of Laboratory Medicine, University Hospitals Leuven, 3000 Leuven, Belgium. [8]Electrophysiology Unit, VIB-KU Leuven Center for Brain & Disease Research, 3000 Leuven, Belgium. [9]VIB Bio Imaging Core, 3000 Leuven, Belgium. [10]Department of Cardiovascular Sciences, KU Leuven, Leuven, Belgium, and Department of Laboratory Medicine, University Hospitals Leuven, 3000 Leuven, Belgium. [11]SYBIOMA, KU Leuven Center for SYstems BIOlogy based MAss spectrometry, 3000 Leuven, Belgium. [12]Laboratory of Tumor Inflammation and Angiogenesis, Center for Cancer Biology, VIB, 3000 Leuven, Belgium. [13]Laboratory of Tumor Inflammation and Angiogenesis, Center for Cancer Biology, Department of Oncology, KU Leuven, 3000 Leuven, Belgium. [14]Metabolomics Expertise Center, Center for Cancer Biology, VIB, KU Leuven, 3000 Leuven, Belgium.
*Corresponding author. Email: pierre.vanderhaeghen@kuleuven.be
†These authors contributed equally to this work.

Mitochondria development during cortical neuronal maturation follows a species-specific timeline

To test whether metabolism influences the species-specific timing of neuronal development, we used in vitro cultures of cortical pyramidal neurons derived from PSCs (human and mouse) or from embryonic brain (mouse), which recapitulate species-specific timelines of corticogenesis (*6*, *24*) (fig. S1A). Given that neurogenesis is not synchronous, it is challenging to study neuronal maturation because populations of neurons born at different time points coexist at the same stage of brain development. To study neuronal development with optimal temporal resolution, we developed a neuronal birth-dating system called neuroD1-dependent newborn neuron (NNN) labeling. NNN combines the expression of tamoxifen-inducible $CreER^{T2}$ (Cre recombinase fused to a mutant estrogen receptor ligand-binding domain) under the control of the promoter of *Neuronal Differentiation 1* (*NeuroD1*), together with the Cre-dependent reporters enhanced green fluorescent protein (eGFP) and truncated CD8, enabling the identification or purification of the labeled cells (Fig. 1A and fig. S1B). Because the *NeuroD1* promoter is turned on transiently at the time of neuron generation, a pulse of 4-hydroxy-tamoxifen (4-OHT) allowed the selective labeling of a cohort of neurons born at precise time points, as assessed by 5-ethynyl-2′-deoxyuridine nuclear labeling (fig. S1, C to E), which revealed a timely progression in growth and complexity (Fig. 1B). To maximize the number of neuronal cells born at similar time points, the cultures were treated simultaneously with the gamma-secretase inhibitor *N*-[*N*-(3,5-difluorophenacetyl)-L-alanyl]-*S*-phenylglycine t-butyl ester (DAPT), which inhibits Notch signaling and thereby increases cortical neurogenesis, and cells were purified by $CD8^+$ magnetic-activated cell sorting (MACS) purification. The purified NNN-labeled neurons thus displayed homogeneous maturation patterns and identity (Fig. 1C and fig. S1, F and G).

To examine mitochondrial dynamics during cortical neuron development, we combined NNN labeling with mitochondria tagging with emerald-green fluorescent protein fused to mitochondrial targeting sequence of cytochrome c oxidase subunit 8A (COX8A) (Fig. 1, D to F). We observed that mitochondria were initially small and sparse in newly born mouse neurons (*20*) and gradually grew in size and quantity over 3 weeks during neuronal maturation, and the same was observed in mouse PSC–derived cortical neurons (Fig. 1, D and F, and fig. S2). However a similar examination of PSC-derived human cortical neurons revealed a more prolonged timeline of mitochondria development, spanning several months (Fig. 1, E and F). We monitored mitochondria dynamics in developing cortical neurons in vivo. We labeled mouse cortical neurons with eGFP by in utero electroporation at embryonic day 14.5 (E14.5), followed by a time course of correlative light and electron microscopy (CLEM) analysis (Fig. 1G and fig. S3A). This confirmed that mitochondria gradually reach maximal levels of growth and size in 3 weeks in mouse cortical neurons in vivo (Fig. 1F). We also xenotransplanted DAPT-treated PSC-derived human cortical neurons transduced with eGFP. In this system, xenotransplanted neurons display a months-long protracted pattern of maturation (*7*). CLEM performed on such neurons revealed slower mitochondria growth than in their mouse counterparts, taking months to reach similar mitochondrial development (Fig. 1H and fig. S3B). We used transmission electron microscopy to visualize mitochondria ultrastructure in greater detail. In newborn neurons, mitochondria were mostly devoid of cristae, whereas there were more, better defined cristae as neurons matured, following a species-specific timeline that was more protracted in human neurons (fig. S3, C and D). Thus, mitochondria morphological development

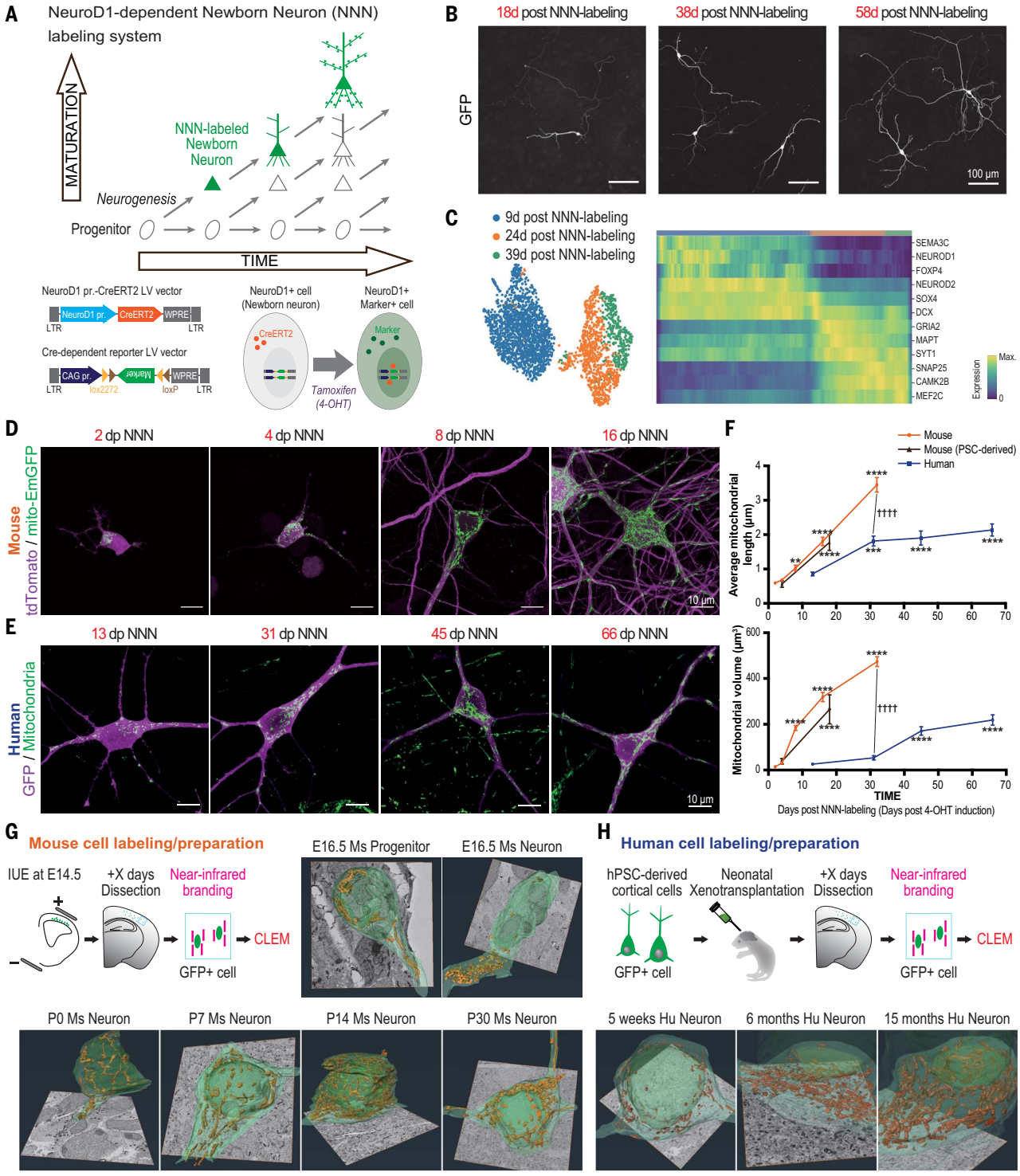

Fig. 1. Interspecies differences in mitochondria biogenesis and dynamics during neuronal development. (**A**) Schematic of the NNN-labeling system. (**B**) Representative images after NNN labeling in human PSC-derived cortical neurons. (**C**) Left: Uniform manifold approximation and projection (UMAP) of MACS-purified NNN-labeled cells. Right: Heatmap of gene expression after pseudotime analysis. (**D** and **E**) Representative images of mitochondrial morphology in NNN-labeled mouse (D) and human (E) neurons. (**F**) Quantification of mitochondrial length (top) and mitochondria volume (bottom) per cell. Mouse: 2, 4, 8, 16, and 32 days post (dp) NNN labeling: length: n = 10, 11, 10, 10, and 5 cells, respectively; volume: n = 6, 8, 10, 9, and 5, respectively. PSC-derived mouse: 4 and 18 dp NNN labeling: length: n = 9 and 9, respectively; volume: n = 9 and 9, respectively. Human: 13, 31, 45, and 66 dp NNN labeling: length: n = 20, 15, 17, and 18, respectively; volume: n = 9, 11, 22, and 20, respectively. (**G** and **H**) Schematic of mouse (Ms) or human (Hu) cortical neuron birth-dating followed by CLEM, and representative images. E, embryonic day; P, postnatal day. Yellow indicates mitochondria. Bottom images are 20 × 20 µm. (F) Data are shown as mean ± SEM. Dunnett's multiple-comparisons test or unpaired t test were used to compare with first time point. Unpaired t test or Mann-Whitney test was used to compare mouse and human. $^{**}P < 0.01$, $^{***}P < 0.001$, $^{****}P < 0.0001$, and ††††$P < 0.0001$.

follows a species-specific timeline that is highly correlated with neuronal maturation.

Mitochondria metabolic activity is lower in human than in mouse developing neurons

We examined the functional properties of mitochondria during neuronal development, focusing on mitochondrial oxidative phosphorylation (OXPHOS) and electron transport chain (ETC) capacity (Fig. 2, A to C). We measured the mitochondrial oxygen consumption rate (OCR) using oxygraphy (*25*) on highly enriched preparations (>95% neurons) of mouse and human cortical neurons at similar time points after birth (fig. S4, A and B). From early stages, mitochondrial OCR was higher in mouse than in human neurons, and also increased more rapidly, which is consistent with their morphological development (Fig. 2, A to C, and fig. S4, C to E). As a result, stimulated OCR was >10 times higher in mouse than in human counterparts after 2 weeks of differentiation (Fig. 2, B and C, and fig. S4). The increased mitochondria ETC activity during mouse neuronal development was confirmed by mitochondria membrane potential measurement using tetramethylrhodamine methyl ester (fig. S5).

We next examined glucose metabolism using mass spectrometry–based ^{13}C tracer analysis (*26*) of enriched preparations of human and mouse developing cortical neurons at similar ages (19 days after neuronal birth) (Fig. 2, D to F, and fig. S6A). Although this led to similar labeling of glycolytic metabolites in the two species, it revealed a higher enrichment of lactate from $^{13}C_6$-glucose and a higher secretion of lactate in human than in mouse neurons (Fig. 2, D to F, and figs. S6 and S7).

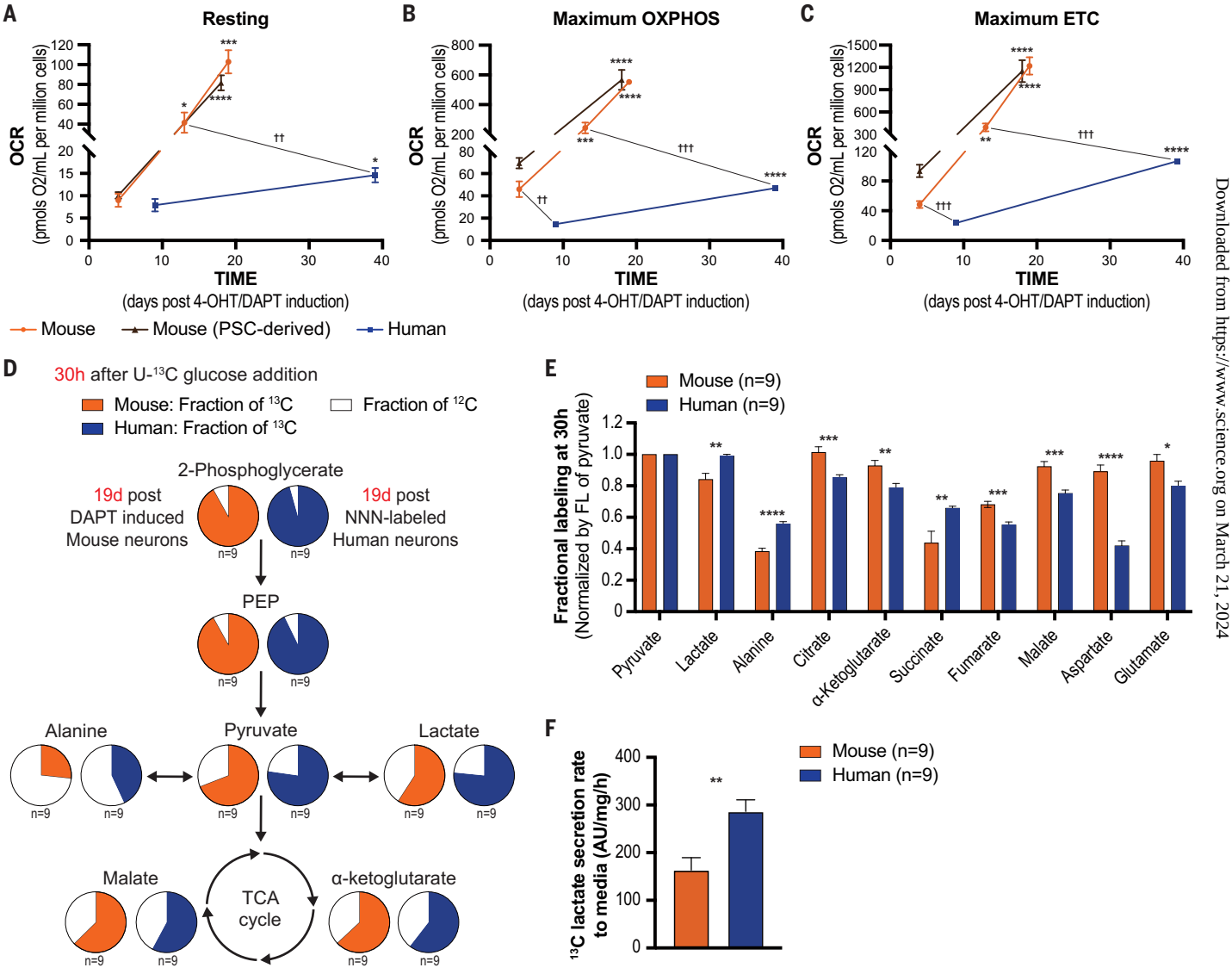

Fig. 2. Interspecies differences in mitochondria metabolism during neuronal development. (**A** to **C**) Quantification of OCR during neuronal development from at least two biological replicates. (A) Resting OCR. (B) Maximum OXPHOS capacity under coupled condition. (C) Maximum ETC capacity under uncoupled condition. Mouse: 4, 13, and 19 dp DAPT induction: n = 6, 8, and 4, respectively. PSC-derived mouse: 4 and 18 dp DAPT induction: n = 14 and 16, respectively. Human: 9 and 37 to 41 dp NNN labeling, n = 6 and 7, respectively. (**D**) ^{13}C enrichment patterns of the metabolites in mouse (orange) and human (blue). PEP, phosphoenolpyruvate. (**E**) Fractional labeling of metabolites normalized by the labeled fraction of pyruvate at 30 hours after tracer addition. (**F**) ^{13}C-labeled lactate secretion rate. AU, arbitrary units. All data are shown as mean ± SEM. For (A) to (C), Dunnett's or Dunn's multiple-comparisons test (mouse) and unpaired t test or Mann-Whitney test (PSC mouse and human) were used to compare with first time point. For (E) and (F), unpaired t test or Mann-Whitney test was used to compare mouse and human. *P < 0.05, **P < 0.01 or ††P < 0.01, ***P < 0.001 or †††P < 0.001, and ****P < 0.0001.

Conversely, the labeling of tricarboxylic acid (TCA) cycle metabolites was comparatively lower in human than in mouse neurons, indicating lower mitochondria metabolic activity (Fig. 2E). Whole-cell oxidized nicotinamide adenine dinucleotide (NAD^+) and reduced NAD (NADH) measurements revealed that the amounts of NAD^+ and NADH were both higher in human neurons, whereas the NAD^+/NADH ratio was similar in both species (fig. S6H). This may suggest a difference in NAD recovery and synthesis between the two species. We also found a higher ratio of reduced glutathione to oxidized glutathione in human neurons (fig. S6D), indicating a lower oxidative stress in human cells consistent with a lower activity of the mitochondrial ETC (Fig. 2C). Adenosine triphosphate (ATP) and adenosine diphosphate (ADP) levels and ATP/ADP ratios were higher in human than in mouse neurons, whereas their fractional labeling from glucose was lower (fig. S6, E and F), suggesting more de novo biosynthesis in mouse neurons.

These data indicate that human developing cortical neurons have lower mitochondria-driven TCA cycle and oxidative activity than do their mouse counterparts at a similar age.

Oxygraphy data point to temporal differences in mitochondrial metabolism during neuronal maturation. To gain insights into what might cause such differences and their in vivo relevance, we examined our single-cell RNA-sequencing data from in vitro birth-dated human neurons with those from human and mouse fetal cortex in vivo (*27*, *28*) (Fig. 3 and figs. S8 to S11). The in vitro and in vivo patterns of expression of mitochondrial or metabolic genes were similar and correlated (Fig. 3, E and F), providing in vivo validation of our in vitro observations. Human and mouse cells had similar temporal patterning of mitochondrial and metabolic genes, with an overall increase in genes related to oxidative phosphorylation and a decrease in genes related to glycolysis, which occurred earlier in mouse than in human neurons (Fig. 3, F and J, and data S2).

Increasing mitochondria activity in human neurons leads to accelerated neuronal maturation

We tested whether the species differences observed in mitochondria metabolic functions could set the speed of neuronal maturation. Glucose tracer experiments revealed an interspecies difference in the conversion of pyruvate to lactate (Fig. 2, D to F), which is catalyzed by lactate dehydrogenase (LDH). LDH is composed of A and B subunits, both of which were expressed in both mouse and human cortical neurons, with higher amounts in human than in mouse (fig. S12).

LDHA favors the conversion of pyruvate to lactate, and LDHB favors the conversion of lactate to pyruvate (*29*) (Fig. 4A). To enhance mitochondria activity in developing neurons, we therefore targeted LDHA. Treatment with a chemical inhibitor of LDHA, GSK-2837808A (hereafter referred to as GSK) (*30*), resulted in increased mitochondria OCR in human neurons (Fig. 4B and fig. S13), consistent with earlier reports (*31*). Similarly, exposure of cells to free fatty acids (AlbuMAX), a fuel in addition to glucose for mitochondrial TCA cycle activity, led to increased OCR, as did its combination with GSK (referred to as AlbuMAX-GSK) (Fig. 4B and fig. S13). These treatments, alone or in combination, led to increased OCR, but not to the level found in mouse neurons (compare Fig. 2, A to C, with Fig. 4B), even with higher concentrations of GSK (fig. S14).

We examined the impact of AlbuMAX-GSK treatment on mitochondria morphology and protein composition. Morphology analyses did not reveal significant effects on mitochondria length and volume (fig. S16, F to H). Western blot analyses did not reveal changes in most tested mitochondria proteins, but some key components were increased in abundance after the treatment, specifically COXII, a component of complex IV (fig. S17). The effects of AlbuMAX-GSK treatments on OCR could still be detected at similar levels of magnitude 1 to 5 days after stopping the treatment (fig. S15). Thus, there appears to be selective molecular and metabolic effects of LDH inhibition leading to increased OXPHOS, rather than global effects on mitochondria biogenesis or dynamics. This could contribute to the observed limits of the effects obtained after manipulations of mitochondria function in human neurons, which never reached the levels found in mouse neurons. None of the treatments enhancing mitochondria appeared to cause changes in neuronal identity or survival, because the amounts of apoptosis remained low and identity marker expression was unchanged after AlbuMAX-GSK treatments (figs. S13G and S16, A to E).

We tested the impact of these treatments on neuronal developmental rates. To determine the speed of maturation, we assessed neuronal excitability by measuring the response of neurons to membrane depolarization induced by the addition of KCl using as a readout the expression of the activity-dependent immediate-early gene *Neuronal PAS Domain Protein 4* (*NPAS4*) (*32*). Few NNN-labeled human cortical neurons responded to KCl shortly after their birth (9 to 24 days), but most of them became responsive weeks later (39 days) (Fig. 4C and fig. S13E). We then examined the impact of LDHA inhibitors on human cortical neuron maturation by treating the cells from day 9 to 23, when the neurons were still poorly responsive to KCl (Fig. 4D and fig. S13F). LDHA inhibitor treatment was stopped for 1 to 5 days before assessing maturation to distinguish the effects on neuronal development from an acute impact on mitochondria function (Fig. 4, D and E, and fig. S15). Few untreated neurons responded to KCl treatment, but inhibition of LDHA increased the proportion of neurons displaying NPAS4 responses (Fig. 4D), indicating acceleration of neuronal maturation in response to increased mitochondrial respiration (Fig. 4B). Increased neuronal maturation was also observed with other treatments that enhance mitochondrial metabolism, including AlbuMAX and PS10, a pyruvate dehydrogenase (PDH) kinase (PDK1-4) inhibitor (*33*) that increases the conversion of pyruvate into acetyl-CoA. The effects of AlbuMAX and GSK were additive (Fig. 4, D and E), further linking mitochondrial metabolic activity to the speed of neuronal maturation. These experiments were performed on human cortical neurons cultured on mouse astrocytes, but a similar acceleration was observed after the same treatment on pure neuronal populations (figs. S13, H to J, S14, C to E, and S15, C to E).

Increased mitochondrial activity appears to lead to accelerated neuronal differentiation. We tested this further by performing patch-clamp recordings of human cortical neurons after AlbuMAX-GSK treatment. This resulted in an increased frequency and amplitude of synaptic currents (Fig. 4, H and I), together with a decrease of membrane potential (fig. S18), consistent with a global increase in the functional maturation of the treated neurons. We also found an increased number of puncta containing the presynaptic marker synapsin I on dendrites of treated neurons (Fig. 4, F and G). The density of synapsin I puncta in 24-day-old treated human neurons was still lower than that in 13-day-old mouse neurons (fig. S16, J and K).

We examined the consequences of AlbuMAX-GSK treatment on neuronal morphogenesis, a crucial parameter of neuronal maturation. AlbuMAX-GSK–treated human cortical neurons had larger neuronal size and increased dendritic length and complexity (Fig. 5, A and B). The morphology of 24-day-old AlbuMAX-GSK–treated neurons reached the same maturation level as for 58-day-old control neurons (Figs. 1B and 5A), indicating that enhanced mitochondrial metabolism could accelerate neuronal morphological development several weeks ahead of time.

To explore the relevance of these observations across species, we tested the influence of mitochondria activity on rates of mouse neuron maturation. Treatment of mouse neurons with AlbuMAX-GSK resulted in increased dendritic growth, although to a lesser extent than in human neurons (Fig. 5, C and D). Reduction of mitochondria activity using either 2-cyano-3-(1-phenyl-1H-indol-e-yl)-2-peopenoic acid (UK-5099) as a mitochondrial pyruvate carrier inhibitor or rotenone as an ETC complex I

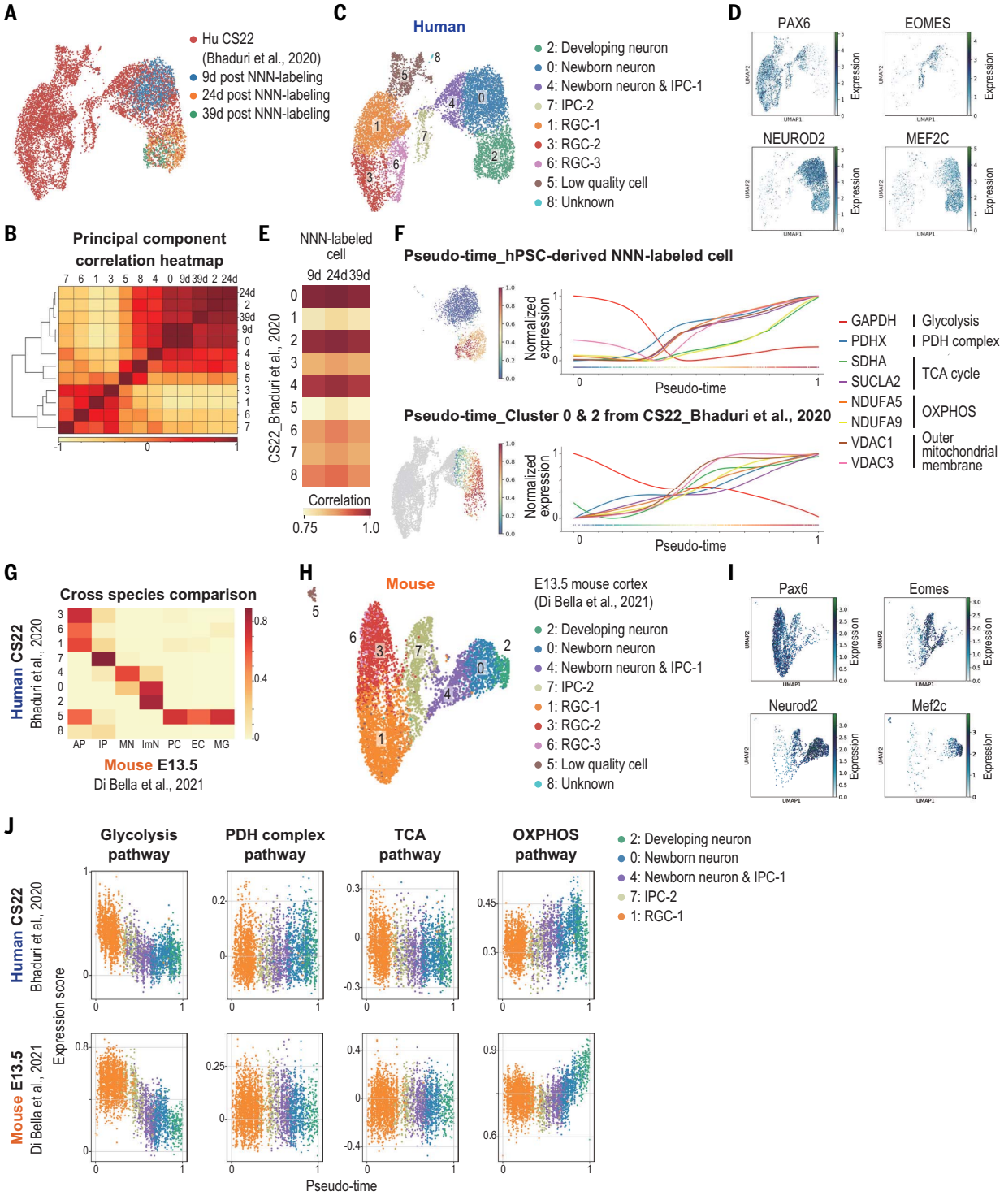

Fig. 3. Temporal pattern of expression of metabolic genes during neuronal development. (**A** to **C**) UMAP of NNN-labeled human cortical neurons and human cortical cells from Carnegie stage (CS) 22 (*27*). (B) Principal component correlation heatmap. (C) Unsupervised Leiden clustering and classification of cells after integration with Harmony algorithm. (**D**) Normalized expressions of PAX6, EOMES, NEUROD2, and MEF2C are shown as radial glial cells (RGCs), intermediate progenitor cells (IPCs), excitatory neurons, and developing neuron markers, respectively. (**E**) Heatmap of Pearson correlation coefficients per time point of the mean scores of metabolic pathways (glycolysis, PDH complex, TCA, and OXPHOS; table S1). (**F**) Expression trends of representative metabolic pathway genes plotted along the pseudotime axis for NNN-labeled neurons (top) and CS22 neurons (bottom) from cluster 0 and 2. (**G**) Heatmap of cell type alignment scores representing the cross-species comparison of E13.5 mouse and CS22 human using SAMap. (**H**) UMAP of mouse cortical cells showing transferred annotations from merged human cells to the mouse dataset. (**I**) Normalized expressions of Pax6, Eomes, Neurod2, and Mef2c. (**J**) Temporal pattern of metabolic pathway score in CS22 human (top) and E13.5 mouse (bottom).

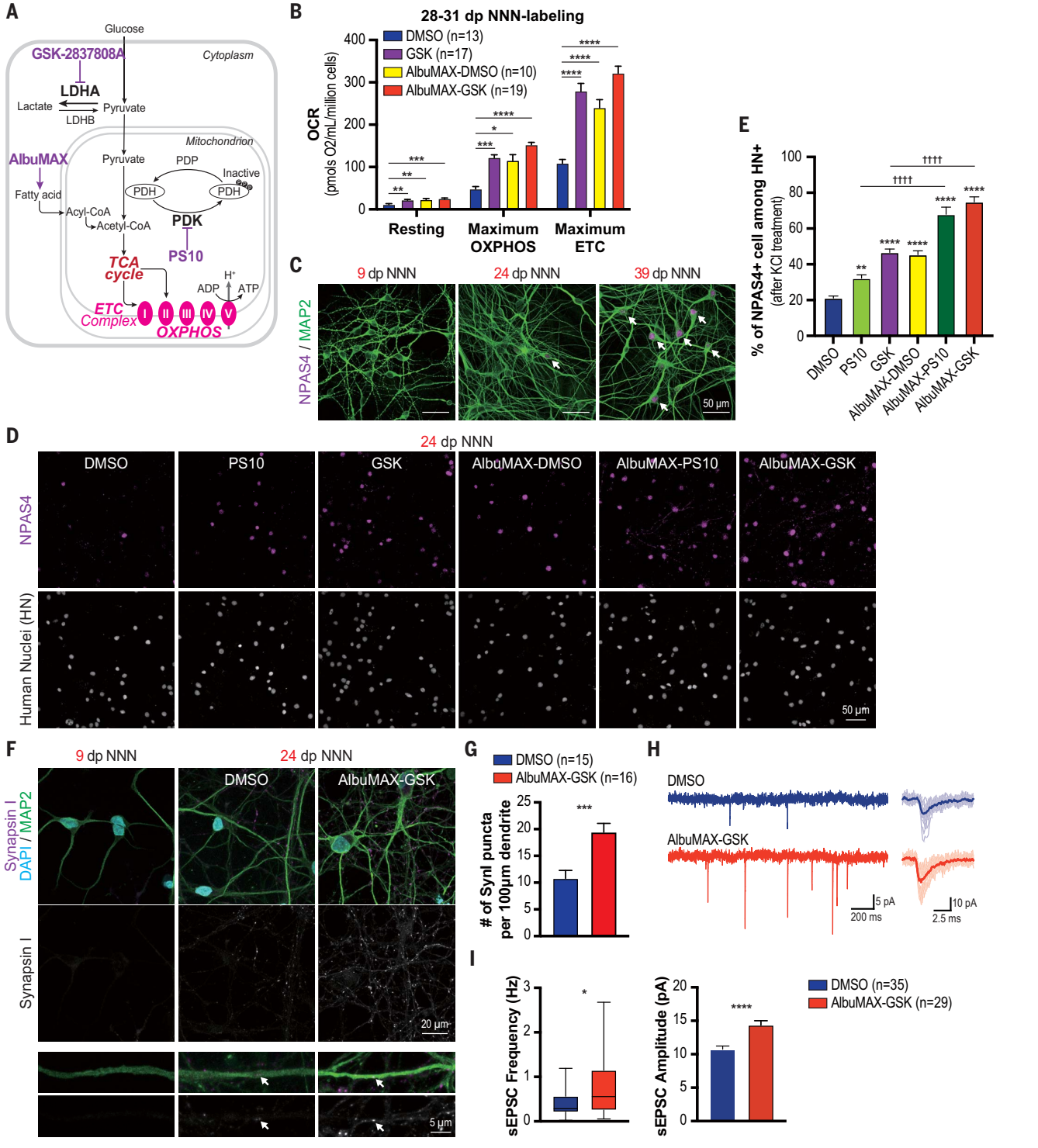

Fig. 4. Increasing mitochondria metabolism accelerates human neuronal maturation. (**A**) Schematic of metabolic pathways targeted by indicated chemical compounds. PDK/*P*, pyruvate dehydrogenase kinase/phosphatase. (**B**) Quantified OCR from 28 to 31 dp NNN-labeled human neurons after treatment with the indicated chemical compounds. (**C**) Representative images of KCl-induced NPAS4 expression in NNN-labeled human neurons over time. Arrow indicates NPAS4+ neurons. (**D** and **E**) Representative images (D) and quantification (E) of NPAS4+ neurons induced by KCl after treatment with the indicated chemical compounds from three independent biological replicates. Dimethylsulfoxide (DMSO): $n = 20$ regions of interest, PS10: $n = 20$, GSK: $n = 15$, AlbuMAX-DMSO: $n = 15$, AlbuMAX-PS10: $n = 10$, and AlbuMAX-GSK: $n = 20$. (**F** and **G**) Representative images (F) and quantification (G) of synapsin I puncta on dendrites from three independent biological replicates. (**H**) Trace of spontaneous excitatory postsynaptic current (sEPSC). (**I**) Quantification of sEPSC frequency (left) and amplitude (right). All data are shown as mean ± SEM as determined by Dunnett's or Dunn's multiple-comparisons test (B); Tukey's multiple-comparisons test (E); unpaired *t* test (G); or unpaired *t* test or Mann-Whitney test (I). $^{*}P < 0.05$, $^{**}P < 0.01$, $^{***}P < 0.001$, $^{****}P < 0.0001$, and ††††$P < 0.0001$.

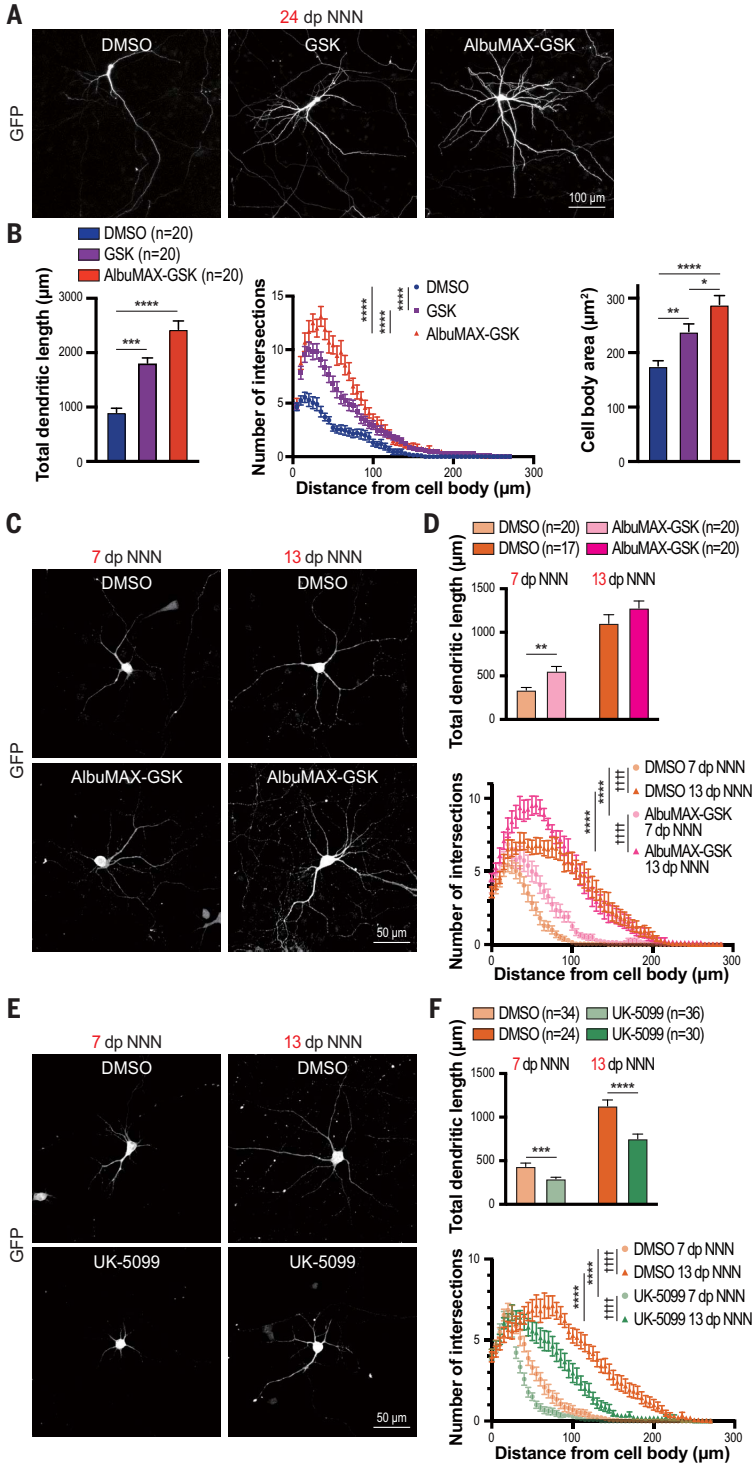

Fig. 5. Functional coupling between mitochondria metabolism and neuronal development across species. (**A** and **B**) Representative images (A) and quantification (B) of NNN-labeled human neurons after the indicated treatments. Left: total dendritic length. Middle: Sholl analysis of dendritic branching. Right: cell body area. (**C** and **E**) Representative images of 7 and 13 dp NNN-labeled mouse neurons after treatment with the indicated chemical compounds. (**D** and **F**) Quantification of total dendritic length (top) and Sholl analysis of dendritic branching (bottom) from three biological replicates. For (A) to (F), data are shown as mean ± SEM by unpaired *t* test, Mann-Whitney test, or Dunn's multiple-comparisons test for dendritic length. Two-way ANOVA test was used for Sholl analysis. Tukey's multiple-comparisons test was used for cell body area. **P* < 0.05, ***P* < 0.01, ****P* < 0.001, *****P* < 0.0001, ††††*P* < 0.0001.

inhibitor resulted in decreased dendritic growth, consistent with slower developmental rates (Fig. 5, E and F, and fig. S19).

We tested whether similar effects could be observed in vivo using xenotransplantation of human cortical neurons in the mouse neonatal cortex (*6*–*8*). We performed genetic manipulation of human neuron metabolism by lentiviral overexpression of LDHB or eGFP as a control. LDHB overexpression led to increased neuronal mitochondria OCR in vitro, as expected (Fig. 6A and fig. S20). We xenotransplanted the transduced neurons, which revealed an increased dendritic length and complexity 4 weeks after transplantation (Fig. 6, B to D), corresponding to a pattern found at 2 to 3 months in control conditions (*7*). Functionality was not tested, but these data indicate that increasing mitochondria metabolic activity results in the acceleration of morphological differentiation of human neurons in vivo.

Discussion

We found that mitochondrial metabolic activity sets the species-specific tempo of development of cortical neurons. Enhanced mitochondria metabolism leads to global acceleration of morphological and functional neuron maturation, but it remains to be determined how much it leads to transcriptional, epigenetic, and proteomic changes in developing neurons. AlbuMAX-GSK–treated neurons were still less mature than mouse counterparts at the same age, indicating that other mechanisms contribute to species differences in neuronal developmental timing, including human-specific genes (*34*), RNA or protein turnover (*35*, *36*), and chromatin remodeling (*37*, *38*).

Our transcriptomic analyses suggest that at least part of the temporal differences in mitochondria maturation originate from patterns of mitochondria gene-regulatory mechanisms, but the observed species differences in mitochondria function likely also involve posttranslational mechanisms such as modifications of mitochondrial dynamics and assembly of the ETC (*39*, *40*).

Differences in species-specific metabolic properties of cortical neurons may influence human brain neoteny, which is consistent with previous reports of years-long periods of aerobic glycolysis in the developing human cortex (*41*). Aerobic glycolysis has long been thought to constitute a hallmark of cellular proliferation, as during oncogenesis (*42*). Here, we found that mitochondrial OXPHOS activity influences the speed of postmitotic neuron morphological and functional development and displays species differences. However, alterations in the TCA cycle or other, yet to be explored metabolic pathways may also contribute to determine the timing of neuronal development.

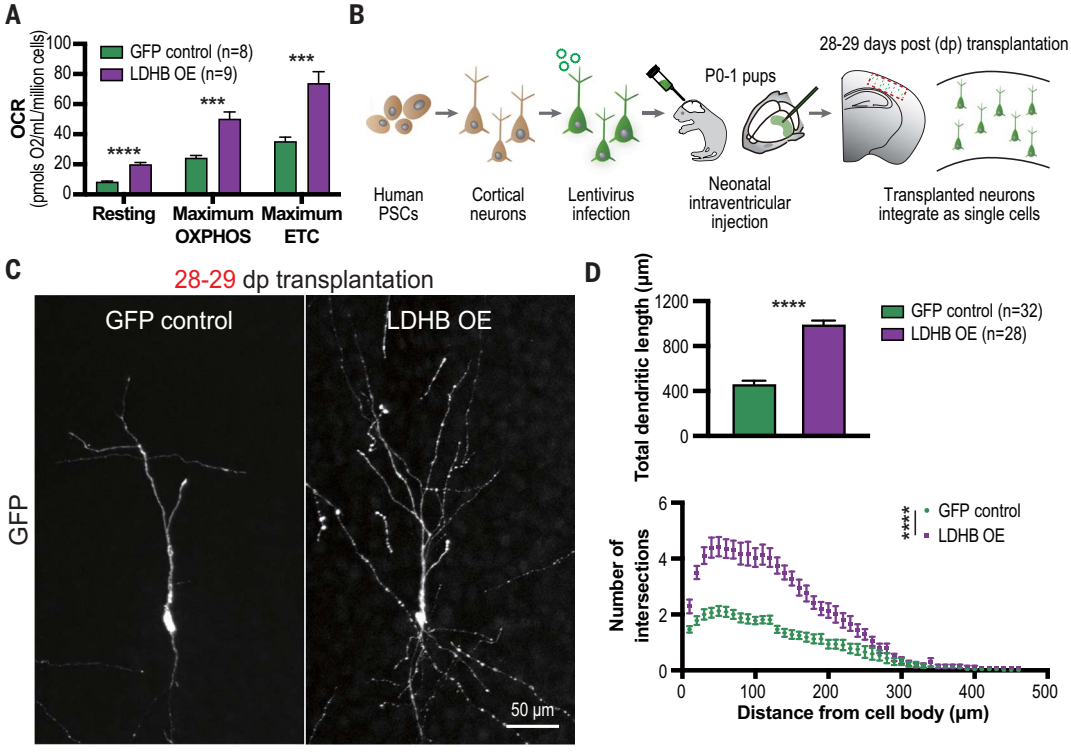

Fig. 6. In vivo maturation of human cortical neurons is enhanced by increased mitochondria function. (**A**) Quantified OCR from three biological replicate experiments. (**B** and **C**) Experimental scheme (B) and representative images (C) of human neurons in mouse cortex at 28 to 29 dp transplantation. (**D**) Quantification of total dendritic length (top) and Sholl analysis of dendritic branching (bottom). All data are shown as mean ± SEM by unpaired *t* test (A). (D) Unpaired *t* test was used for dendritic length. Two-way ANOVA test was used for Sholl analysis. ***$P < 0.001$, ****$P < 0.0001$.

The temporal patterning of mitochondria development is likely an important contributor to the observed species differences in metabolic activity. However, the differences observed in mitochondria function at early stages of neuronal development also suggest that mitochondria from different species may display quantitative or qualitative differences independently of their developmental patterns. This will be important to resolve, because mitochondria and metabolism could contribute to developmental timing in other contexts, from the speed of the somitic clock (*43*) to the maturation of cardiac and pancreas cells (*13*–*15*).

Accelerated human neuronal maturation in vitro might benefit PSC-based modeling of neural diseases, which remains greatly hindered by the slowness of human neuron development. Conversely, human neuronal prolonged development has been long proposed to have a positive role in acquiring human-specific cognitive features (*5*). Tools to accelerate or decelerate neuronal development could allow testing of the impact of neuronal neoteny on brain function, plasticity, and disease.

Materials and methods summary

Detailed information on all materials and methods performed are provided in the supplementary materials.

NeuroD1-dependent NN labeling and purification

Human cortical cell culture was performed as described previously (*20*). Dissociated cells were transduced with the following lentiviruses: LV-NeuroD1 promoter-CreERT2-WPRE and LV-CAG-DIO-Reporter (EGFP and/or truncated CD8)-WPRE. For Cre-dependent recombination, 4-OHT (final concentration: 0.25 µM) was added to the medium for 48 hours. For purification of newborn neurons, cortical cells were dissociated using the NeuroCult Enzymatic Dissociation Kit (STEMCELL Technologies) 48 hours after withdrawal of 4-OHT. The dissociated cells were incubated with magnetic bead–conjugated antihuman CD8 (Miltenyi Biotec) in MACS buffer (Miltenyi Biotec). $CD8^+$ selection was performed with LS columns (Miltenyi Biotec). The sorted cells were plated on mouse astrocyte–coated or poly-L-ornithine-/laminin–coated plates.

Oxygraphy

Cells were dissociated using the NeuroCult Enzymatic Dissociation Kit and resuspended in MiR05 buffer (Oroboros Ecosystem). The cell suspension was injected in a chamber of oxygraphy O2K with subsequent injections of the following chemical compounds to final concentrations as follows (all from Merck except for ADP, which was from Calbiochem): 556 U/ml catalase, 10 µg/ml digitonin, 5 mM pyruvate, 0.5 mM malate, 1 mM ADP, 10 mM glutamate, 10 mM succinate, carbonyl cyanide *m*-chlorophenyl hydrazone (CCCP) Δ1 µM until maximum respiration reached, 75 nM rotenone, 10 mM glycerophosphate, 250 nM antimycin A, 2 mM sodium ascorbate, 0.5 mM N,N,N′,N′-tetramethyl-p-phenylenediamine dihydrochloride, 10 µM cytochrome C, and 200 mM sodium azide. The reported values of maximum OXPHOS (phosphorylating) and ETC (nonphosphorylating) were calculated as succinate minus antimycin A (nonmitochondrial respiration) and CCCP minus antimycin A, respectively (*25*).

Metabolic labeling

One day before the glucose-tracing experiment, the medium was exchanged with Neurobasal/B27 (2.5 mM glucose). After one day, the medium was switched to Neurobasal/B27 (2.5 mM U-^{13}C glucose; Cambridge Isotope Laboratories). After 30 hours of incubation, medium and plates were snap-frozen in liquid nitrogen.

Metabolic modulation by chemical compounds

On the first day of the experiment, the culture medium was removed and replaced by Neurobasal/B27 (2.5 mM glucose) with the indicated chemical compounds: GSK-2837808A (1 to 10 µM; MedChemExpress), PS10 (5 µM; MedChemExpress), AlbuMAX (0.5% w/v; Thermo Fisher Scientific), UK-5099 (2.5 µM; Sigma-Aldrich), and rotenone (21 nM; Sigma-Aldrich). Eighty percent of the culture medium was exchanged with fresh medium and compounds every other day.

Xenotransplantation

Human neuron xenotransplantation was performed as described previously (*7*). On the day of xenotransplantation, cortical cells were dissociated using the NeuroCult Enzymatic Dissociation Kit and resuspended in a solution containing 20 mM EGTA (Merck) and

0.1% Fast Green (Merck) in phosphate-buffered saline at 100,000 to 200,000 cells/μl. Approximately 1 to 2 μl of cell suspension was injected into the lateral ventricles of each hemisphere of postnatal day 0 or 1 mouse brains. At the indicated time points, the mice were sacrificed and perfused with the proper fixative.

REFERENCES AND NOTES

1. M. Ebisuya, J. Briscoe, What does time mean in development? *Development* **145**, dev164368 (2018). doi: 10.1242/dev.164368; pmid: 29945985
2. R. Iwata, Temporal differences of neurodevelopment processes between species. *Neurosci. Res.* **177**, 8–15 (2022). doi: 10.1016/j.neures.2021.08.004; pmid: 34419562
3. R. Iwata, P. Vanderhaeghen, Tempus fugit: How time flies during development. *Science* **369**, 1431–1432 (2020). doi: 10.1126/science.abe0953; pmid: 32943512
4. B. Libé-Philippot, P. Vanderhaeghen, Cellular and molecular mechanisms linking human cortical development and evolution. *Annu. Rev. Genet.* **55**, 555–581 (2021). doi: 10.1146/annurev-genet-071719-020705; pmid: 34535062
5. C. C. Sherwood, A. Gomez-Robles, Brain plasticity and human evolution. *Annu. Rev. Anthropol.* **46**, 399–419 (2017). doi: 10.1146/annurev-anthro-102215-100009
6. I. Espuny-Camacho *et al*., Pyramidal neurons derived from human pluripotent stem cells integrate efficiently into mouse brain circuits in vivo. *Neuron* **77**, 440–456 (2013). doi: 10.1016/j.neuron.2012.12.011; pmid: 23395372
7. D. Linaro *et al*., Xenotransplanted human cortical neurons reveal species-specific development and functional integration into mouse visual circuits. *Neuron* **104**, 972–986.e6 (2019). doi: 10.1016/j.neuron.2019.10.002; pmid: 31761708
8. M. C. Marchetto *et al*., Species-specific maturation profiles of human, chimpanzee and bonobo neural cells. *eLife* **8**, e37527 (2019). doi: 10.7554/eLife.37527; pmid: 30730291
9. M. Knobloch, S. Jessberger, Metabolism and neurogenesis. *Curr. Opin. Neurobiol.* **42**, 45–52 (2017). doi: 10.1016/j.conb.2016.11.006; pmid: 27915086
10. N. Shyh-Chang, G. Q. Daley, L. C. Cantley, Stem cell metabolism in tissue development and aging. *Development* **140**, 2535–2547 (2013). doi: 10.1242/dev.091777; pmid: 23715547
11. L. Pernas, L. Scorrano, Mito-morphosis: Mitochondrial fusion, fission, and cristae remodeling as key mediators of cellular function. *Annu. Rev. Physiol.* **78**, 505–531 (2016). doi: 10.1146/annurev-physiol-021115-105011; pmid: 26667075
12. O. A. Tarazona, O. Pourquié, Exploring the influence of cell metabolism on cell fate through protein post-translational modifications. *Dev. Cell* **54**, 282–292 (2020). doi: 10.1016/j.devcel.2020.06.035; pmid: 32693060
13. X. Yang *et al*., Fatty acids enhance the maturation of cardiomyocytes derived from human pluripotent stem cells. *Stem Cell Reports* **13**, 657–668 (2019). doi: 10.1016/j.stemcr.2019.08.013; pmid: 31564645
14. D. Hu *et al*., Metabolic maturation of human pluripotent stem cellderived cardiomyocytes by inhibition of HIF1α and LDHA. *Circ. Res.* **123**, 1066–1079 (2018). doi: 10.1161/CIRCRESAHA.118.313249; pmid: 30355156
15. E. Yoshihara *et al*., ERRγ is required for the metabolic maturation of therapeutically functional glucose-responsive β cells. *Cell Metab.* **23**, 622–634 (2016). doi: 10.1016/j.cmet.2016.03.005; pmid: 27076077
16. Z. Li, K. Okamoto, Y. Hayashi, M. Sheng, The importance of dendritic mitochondria in the morphogenesis and plasticity of spines and synapses. *Cell* **119**, 873–887 (2004). doi: 10.1016/j.cell.2004.11.003; pmid: 15607982
17. P. Licznerski *et al*., ATP synthase c-subunit leak causes aberrant cellular metabolism in fragile X syndrome. *Cell* **182**, 1170–1185.e9 (2020). doi: 10.1016/j.cell.2020.07.008; pmid: 32795412
18. V. Rangaraju, M. Lauterbach, E. M. Schuman, Spatially stable mitochondrial compartments fuel local translation during plasticity. *Cell* **176**, 73–84.e15 (2019). doi: 10.1016/j.cell.2018.12.013; pmid: 30612742
19. K. Steib, I. Schäffner, R. Jagasia, B. Ebert, D. Chichung Lie, Mitochondria modify exercise-induced development of stem cell-derived neurons in the adult brain. *J. Neurosci.* **34**, 6624–6633 (2014). doi: 10.1523/JNEUROSCI.4972-13.2014; pmid: 24806687
20. R. Iwata, P. Casimir, P. Vanderhaeghen, Mitochondrial dynamics in postmitotic cells regulate neurogenesis. *Science* **369**, 858–862 (2020). doi: 10.1126/science.aba9760; pmid: 32792401
21. R. Iwata, P. Vanderhaeghen, Regulatory roles of mitochondria and metabolism in neurogenesis. *Curr. Opin. Neurobiol.* **69**, 231–240 (2021). doi: 10.1016/j.conb.2021.05.003; pmid: 34171617
22. D. S. Glazier, Is metabolic rate a universal 'pacemaker' for biological processes? *Biol. Rev. Camb. Philos. Soc.* **90**, 377–407 (2015). doi: 10.1111/brv.12115; pmid: 24863680
23. G. B. West, J. H. Brown, B. J. Enquist, A general model for ontogenetic growth. *Nature* **413**, 628–631 (2001). doi: 10.1038/35098076; pmid: 11675785
24. N. Gaspard *et al*., An intrinsic mechanism of corticogenesis from embryonic stem cells. *Nature* **455**, 351–357 (2008). doi: 10.1038/nature07287; pmid: 18716623
25. M. J. Bird *et al*., Oxygraphy versus enzymology for the biochemical diagnosis of primary mitochondrial disease. *Metabolites* **9**, 220 (2019). doi: 10.3390/metabo9100220; pmid: 31658717
26. J. M. Buescher *et al*., A roadmap for interpreting (13)C metabolite labeling patterns from cells. *Curr. Opin. Biotechnol.* **34**, 189–201 (2015). doi: 10.1016/j.copbio.2015.02.003; pmid: 25731751
27. A. Bhaduri *et al*., Cell stress in cortical organoids impairs molecular subtype specification. *Nature* **578**, 142–148 (2020). doi: 10.1038/s41586-020-1962-0; pmid: 31996853
28. D. J. Di Bella *et al*., Molecular logic of cellular diversification in the mouse cerebral cortex. *Nature* **595**, 554–559 (2021). doi: 10.1038/s41586-021-03670-5; pmid: 34163074
29. C. J. Valvona, H. L. Fillmore, P. B. Nunn, G. J. Pilkington, The regulation and function of lactate dehydrogenase A: Therapeutic potential in brain tumor. *Brain Pathol.* **26**, 3–17 (2016). doi: 10.1111/bpa.12299; pmid: 26269128
30. J. Billiard *et al*., Quinoline 3-sulfonamides inhibit lactate dehydrogenase A and reverse aerobic glycolysis in cancer cells. *Cancer Metab.* **1**, 19 (2013). doi: 10.1186/2049-3002-1-19; pmid: 24280423
31. V. R. Fantin, J. St-Pierre, P. Leder, Attenuation of LDH-A expression uncovers a link between glycolysis, mitochondrial physiology, and tumor maintenance. *Cancer Cell* **9**, 425–434 (2006). doi: 10.1016/j.ccr.2006.04.023; pmid: 16766262
32. D. H. Ebert, M. E. Greenberg, Activity-dependent neuronal signalling and autism spectrum disorder. *Nature* **493**, 327–337 (2013). doi: 10.1038/nature11860; pmid: 23325215
33. S. C. Tso *et al*., Structure-guided development of specific pyruvate dehydrogenase kinase inhibitors targeting the ATP-binding pocket. *J. Biol. Chem.* **289**, 4432–4443 (2014). doi: 10.1074/jbc.M113.533885; pmid: 24356970
34. C. Charrier *et al*., Inhibition of SRGAP2 function by its human-specific paralogs induces neoteny during spine maturation. *Cell* **149**, 923–935 (2012). doi: 10.1016/j.cell.2012.03.034; pmid: 22559944
35. M. Matsuda *et al*., Species-specific segmentation clock periods are due to differential biochemical reaction speeds. *Science* **369**, 1450–1455 (2020). doi: 10.1126/science.aba7668; pmid: 32943519
36. T. Rayon *et al*., Species-specific developmental timing is associated with global differences in protein stability in mouse and human. *Science* **3**, (2020). doi: 10.1101/2019.12.29.889543
37. G. Ciceri *et al*., An epigenetic barrier sets the timing of human neuronal maturation. bioRxiv 490114 (2022); https://doi.org/10.1101/2022.06.02.490114.
38. Q. Wu *et al*., Selective translation of epigenetic modifiers affects the temporal pattern and differentiation of neural stem cells. *Nat. Commun.* **13**, 470 (2022). doi: 10.1038/s41467-022-28097-y; pmid: 35078993
39. S. Cogliati, J. L. Cabrera-Alarcón, J. A. Enriquez, Regulation and functional role of the electron transport chain supercomplexes. *Biochem. Soc. Trans.* **49**, 2655–2668 (2021). doi: 10.1042/BST20210460; pmid: 34747989
40. M. Giacomello, A. Pyakurel, C. Glytsou, L. Scorrano, The cell biology of mitochondrial membrane dynamics. *Nat. Rev. Mol. Cell Biol.* **21**, 204–224 (2020). doi: 10.1038/s41580-020-0210-7; pmid: 32071438
41. M. S. Goyal, M. Hawrylycz, J. A. Miller, A. Z. Snyder, M. E. Raichle, Aerobic glycolysis in the human brain is associated with development and neotenous gene expression. *Cell Metab.* **19**, 49–57 (2014). doi: 10.1016/j.cmet.2013.11.020; pmid: 24411938
42. M. G. Vander Heiden, L. C. Cantley, C. B. Thompson, Understanding the Warburg effect: The metabolic requirements of cell proliferation. *Science* **324**, 1029–1033 (2009). doi: 10.1126/science.1160809; pmid: 19460998
43. M. Diaz-Cuadros *et al*., Metabolic regulation of species-specific developmental rates. *Nature* **613**, 550–557 (2023).

ACKNOWLEDGMENTS

We thank the members of P.Va.'s laboratory and F. Polleux for helpful discussions and valuable help. **Funding:** This work was funded by the European Research Council (NEUROTEMPO), the EOS Programme PANDAROME, the Belgian FWO and FRS/FNRS, the Generet Fund (P.Va.), the Belgian Queen Elizabeth Foundation (to R.I. and P.Va.). The authors gratefully acknowledge the VIB Bio Imaging Core for support and assistance in this work. R.I. was supported by a postdoctoral fellowship from the FRS/FNRS. P.C. holds a PhD fellowship of the FWO. L.B. holds a fellowship of the FWO. A.V. holds a PhD fellowship of the FWO (file no. 1176821N). P.Ve. is a senior clinical investigator of the FWO. S.M.F. acknowledges funding from the ERC (ERC Consolidator grant no. 771486–MetaRegulation), FWO, Fonds Baillet Latour, KU Leuven (FTBO and internal funding), and King Baudouin. **Author contributions:** Conceptualization: R.I., P.C., P.Va.; Formal analysis: R.I., P.C., E.E., N.C., S.P., P.Ve., B.G., K.D., B.G., S.M.F., S.C., K.W., P.Va.; Funding acquisition: P.Va.; Investigation: R.I., P.C., E.E., L.B., M.M., M.B., I.G.L., M.D., S.P., B.G., S.E., V.G., S.B., A.V., D.R., N.G., S.C., I.V., E.C., K.W., S.M.F., P.Va.; Methodology: R.I., P.C., P.Va.; Resources: P.Ve., S.A., P.Va.; Supervision: P.Va.; Writing: R.I., P.C., P.Va. **Competing interests:** The authors declare no competing interests. **Data and materials availability:** All data are available in the manuscript or the supplementary materials. All materials are available upon request from P.Va. The single-cell RNA-sequencing data reported in this paper are accessible on NCBI's Gene Expression Omnibus (GEO accession number GSE219253).

SUPPLEMENTARY MATERIALS

science.org/doi/10.1126/science.abn4705
Materials and Methods
Figs. S1 to S20
Table S1
References (*44*–*55*)
Data S1 and S2
MDAR Reproducibility Checklist

View/request a protocol for this paper from *Bio-protocol*.

Submitted 3 December 2021; resubmitted 19 August 2022
Accepted 10 January 2023
Published online 26 January 2023
10.1126/science.abn4705